THE JOURNAL OF PHYSICAL CHEMISTRY A

Article

Cite This: J. Phys. Chem. A 2018, 122, 1886−1895

pubs.acs.org/JPCA

Benchmark ab Initio Characterization of the Complex Potential Energy Surfaces of the X^- + NH_2Y [X, Y = F, Cl, Br, I] Reactions

Bálint Hajdu and Gábor Czakó*

Department of Physical Chemistry and Materials Science, Institute of Chemistry, University of Szeged, Rerrich Béla tér 1, Szeged H-6720, Hungary

Supporting Information

ABSTRACT: We report a comprehensive high-level explicitly correlated ab initio study on the X^- + NH_2Y [X,Y = F, Cl, Br, I] reactions characterizing the stationary points of the S_N2 (Y^- + NH_2X) and proton-transfer (HX + NHY^-) pathways as well as the reaction enthalpies of various endothermic additional product channels such as H^- + NHXY, XY^- + NH_2, XY + NH_2^-, and XHY^- + NH. Benchmark structures and harmonic vibrational frequencies are obtained at the CCSD(T)-F12b/aug-cc-pVTZ(-PP) level of theory, followed by CCSD(T)-F12b/aug-cc-pV*n*Z(-PP) [*n* = Q and 5] and core correlation energy computations. In the entrance and exit channels we find two equivalent hydrogen-bonded C_1 minima, X^-···HH′NY and X^-···H′HNY connected by a C_s first-order saddle point, X^-···H_2NY, as well as a halogen-bonded front-side complex, X^-···YNH_2. S_N2 reactions can proceed via back-side attack Walden inversion and front-side attack retention pathways characterized by first-order saddle points, submerged [X−NH_2−Y]$^-$ and high-energy [H_2NXY]$^-$, respectively. Product-like stationary points below the HX + NHY^- asymptotes are involved in the proton-transfer processes.

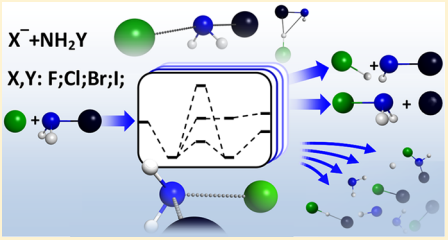

I. INTRODUCTION

The bimolecular nucleophilic substitution (S_N2) processes play a central role in chemistry from the basic understanding of chemical reaction mechanisms to synthetic applications. S_N2 reactions usually occur at carbon (C) centers, where a new bond forms between the nucleophile (X^-) and the C atom while a CY bond breaks heterolytically forming Y^-, where X and Y can be F, Cl, Br, I, OH, CN, NH_2, etc., and the configuration around the C atom gets inverted. This is the famous Walden-inversion mechanism of S_N2 reactions, discovered experimentally more than a hundred years ago[1] and explained at the atomic level in the first half of the 20th century.[2] Despite the long history of and extensive research on S_N2 reactions, many new and sometimes surprising findings have been uncovered for simple S_N2 systems in the 21st century.[3−11] For example, in 2008 Wester and co-workers developed a novel crossed-beam technique for imaging S_N2 reaction dynamics.[5] The crossed-beam experiments complemented with direct dynamics simulations revealed a new roundabout mechanism for the Cl^- + CH_3I S_N2 reaction[5] and several direct and indirect, complex-forming reaction pathways for F^- + CH_3I.[12] In 2013 we reported the first chemically accurate full-dimensional ab initio potential energy surface (PES) for the F^- + CH_3Cl reaction[13] followed by an improved global PES for F^- + CH_3Cl[6] and similar high-level PESs for the F^- + CH_3F and CH_3I systems.[14,15] Reaction dynamics simulations on these PESs revealed a new double-inversion mechanism,[6] leaving group effect,[7] and front-side complex formation[8] in S_N2 reactions. Furthermore, we recently reported benchmark ab initio data for several S_N2 reactions describing novel stationary points and using techniques beyond the standard correlation methods.[16,17]

S_N2 reactions cannot just occur at carbon centers. For example, nitrogen-centered S_N2 reactions can also proceed via the above-described Walden-inversion pathway. Besides the C-centered reactions, there has been considerable interest in studying the kinetics, dynamics, and mechanisms of the N-centered S_N2 reactions.[18−29] Following the early work,[18] in 1995 Radom and co-workers[19] reported a "high-level computational study" on the ab initio characterization of the PESs of the X^- + NH_2X [X = F, Cl, Br, I] S_N2 reactions. At that time high-level meant the use of a modified G2 composite method, G2(+), based on MP2/double-ζ geometries and frequencies and QCISD(T)/triple-ζ energies.[19] The G2(+) method was also used in 2004 by Ren and Zhu[22] to study the nonidentity reactions of X^- + $N(CH_3)_2Y$ [X,Y = F, Cl, Br, I]. Furthermore, several density functional theory (DFT) studies were reported to characterize the PESs of the identity (X = Y) and nonidentity (X ≠ Y) X^- + NH_2Y reactions.[21,23,27] Besides the static electronic structure studies, the dynamics of the OH^- + NH_2Y [Y = F, Cl] (MP2(full)/6-31+G(d)),[24] F^- + NH_2F (MP2/6-31+G(d,p)),[25] and F^- + NH_2Cl (B3LYP/aug-cc-pVDZ)[28] S_N2 reactions were investigated using the direct dynamics method with the electronic structure level indicated in parentheses. Arriving to the recent years, in 2016 Liu et al.[27] reported an ab initio study for the F^- + NH_2Cl reaction computing MP2/aug-cc-pVDZ geometries and CCSD(T)/complete-basis-set energies using the aug-cc-pV*n*Z [*n* = 2−5] basis sets and in the same year Wang and co-workers[26] characterized

Received: December 3, 2017
Revised: January 15, 2018
Published: January 23, 2018

DOI: 10.1021/acs.jpca.7b11927
J. Phys. Chem. A 2018, 122, 1886−1895

the $OH^- + NH_2Cl$ reaction in water. In 2017 Kubelka and Bickelhaupt[29] performed an activation strain analysis for $Cl^- + NH_2Cl$ and Liu et al.[28] reported the above-mentioned direct dynamics study for $F^- + NH_2Cl$.

In the present study we focus on the identity and nonidentity $X^- + NH_2Y$ [X,Y = F, Cl, Br, I] reactions. As discussed above most of the previous N-centered S_N2 studies provided MP2 or DFT geometries with double-ζ-quality basis sets, used standard correlation methods, and focused on a few systems. Here, we report a comprehensive high-level ab initio characterization of the PESs of the $X^- + NH_2Y$ [X,Y = F, Cl, Br, I] reactions utilizing (a) the novel explicitly correlated CCSD(T)-F12b method[30] for the structures, frequencies, and energies and (b) the aug-cc-pV*n*Z(-PP) [n = 2−5] basis sets[31,32] with relativistic effective core potentials[32] for Br and I, and considering (c) the core electron correlation effects. Furthermore, besides the S_N2 channel, we describe several product channels leading to HX + NHY^-, $H^- + NHXY$, $XY^- + NH_2$, $XY + NH_2^-$, and $XHY^- + NH$. The present study aims to provide benchmark stationary-point properties thereby supporting future electronic structure and reaction dynamics investigations. For the latter the development of a full-dimensional ab initio global PES would be desired and the present study may guide such work by anchoring the stationary points and product asymptotes of the PES. We describe the computational details in section II and discuss the results in section III. The paper ends with summary and conclusions in section IV.

II. COMPUTATIONAL DETAILS

All the stationary points of the $X^- + NH_2Y$ [X,Y = F, Cl, Br, I] systems are preoptimized using the second-order Møller−Plesset [MP2] method[33] with the augmented correlation-consistent polarized-valence-double-ζ [aug-cc-pVDZ(-PP)] basis set,[31,32] followed by explicitly correlated coupled cluster singles, doubles, and perturbative triples [CCSD(T)-F12b][30] geometry and frequency computations with the aug-cc-pVDZ(-PP) and aug-cc-pVTZ(-PP) basis sets. Then, at the CCSD(T)-F12b/aug-cc-pVTZ(-PP) structures single-point frozen-core CCSD(T)-F12b energy computations are performed using the large aug-cc-pVQZ(-PP) and aug-cc-pV5Z(-PP) basis sets and core correlation contributions (Δ_{core}) are determined as differences between all-electron and frozen-core energies obtained at the CCSD(T)/aug-cc-pwCVTZ(-PP) level of theory. For Br and I relativistic effective core potentials replacing the inner-core $1s^22s^22p^6$ and $1s^22s^22p^63s^23p^63d^{10}$ electrons, respectively, and the corresponding pseudopotential (PP) basis sets are used.[32] Frozen-core methods correlate the valence electrons only, whereas in the all-electron computations the $1s^2$ (N and F), $2s^22p^6$ (Cl), $3s^23p^63d^{10}$ (Br), and $4s^24p^64d^{10}$ (I) core electrons are also correlated. For open-shell systems the restricted-MP2 [RMP2],[34] the unrestricted-CCSD(T) [UCCSD(T)],[35] and the UCCSD(T)-F12b[36] methods are used based on restricted open-shell Hartree−Fock [ROHF] orbitals. For all the F12b computations the default auxiliary basis sets are employed for density fitting and resolution of identity, except for Br and I, where default density fitting basis is not defined for the aug-cc-pV5Z-PP orbital basis, thus, aug-cc-pVQZ-PP/MP2FIT is used.

The benchmark classical energies are obtained as

$$E[\text{CCSD(T)-F12b/aug-cc-pV5Z(-PP)}] + \Delta_{core}[\text{CCSD(T)/aug-cc-pwCVTZ(-PP)}] \quad (1)$$

and the best adiabatic energies are determined as

$$E[\text{CCSD(T)-F12b/aug-cc-pV5Z(-PP)}] + \Delta_{core}[\text{CCSD(T)/aug-cc-pwCVTZ(-PP)}] + \text{ZPE}[\text{CCSD(T)-F12b/aug-cc-pVTZ(-PP)}] \quad (2)$$

where ZPE is the zero-point energy correction. Note that in a few cases where the CCSD(T)-F12b/aug-cc-pVTZ(-PP) geometry optimizations do not converge, eq 1 and 2 utilize MP2/aug-cc-pVDZ(-PP) structures and frequencies. All the electronic structure computations are performed using the ab initio program package MOLPRO.[37]

III. RESULTS AND DISCUSSION

The schematic PESs of the identity and nonidentity $X^- + NH_2Y$ [X,Y = F, Cl, Br, I] S_N2 and proton-transfer reactions showing the benchmark classical and adiabatic relative energies of the most relevant stationary points are given in Figures 1 and 2, respectively. The structures of the stationary points showing the most important structural parameters are presented in Figures 3 and 4, where the minima (IMs) and transition states (TSs) of Figures 1 and 2 are complemented with additional stationary points which may play a role in the S_N2 and proton-transfer processes. Tables 1 and 2 show the benchmark relative energies and their components, CCSD(T)-F12b/aug-cc-pV5Z(-PP), Δ_{core}, and Δ_{ZPE}, for all the above-mention stationary points as well as for various high-energy product channels besides the major S_N2 and proton-transfer channels. Furthermore, the interested reader can consult with the detailed Supporting Information, where all the ab initio data including the absolute energies, structural parameters and the corresponding *Z*-matrices as well as the harmonic vibrational frequencies are given.

As shown in Figures 1 and 2 the $X^- + NH_2Y$ [X,Y = F, Cl, Br, I] S_N2 reactions have double-well PESs with deep minima in the reactant (IM1) and product (IM2) valleys and a central transition state (TS1, first-order saddle point with C_s symmetry) separating the two wells. In all cases, TS1 is below the reactant asymptote by 11−14 kcal/mol for X = F and by 1−5 kcal/mol for X = Cl, Br, I. The IM1 minima are around 30 kcal/mol deep, relative to $X^- + NH_2Y$, for X = F, whereas around 15 kcal/mol for X = Cl, Br, I with only 2−3 kcal/mol variance depending on X and Y. IM1 has a hydrogen-bonded (H-bonded) structure (C_1 symmetry); thus, two equivalent IM1 minima exist, depending on which of the two H atoms is connected to X^-. We have found a first-order saddle point (IM1′, C_s symmetry) connecting the two H-bonded minima, see Figure 1, via a barrier of 5−8 kcal/mol for X = F and only around 1 kcal/mol for X = Cl, Br, I. As shown in Figures 3 and 4, the structure of NH_2Y is just slightly perturbed at IM1 and IM1′. At IM1 the X···H bonds are 1.3−1.4 Å for X = F and 2.1, 2.3, and 2.6 Å for X = Cl, Br, and I, respectively. At IM1′ the nucleophile connects symmetrically to the two H atoms with longer X···H distances of 2.0, 2.6, 2.7, and 3.0 Å for X = F, Cl, Br, and I, respectively. The finding that the IM1 is significantly deeper and the barrier between the two IM1 minima is much larger for X = F than for the other halide ions is consistent with the strong H-bond ability of fluorine. In the case of the analogous $X^- + CH_3Y$ S_N2 reactions, H-bonded complexes were also found for X = F,[10,11] albeit their stability is roughly half of the corresponding F^-···HHNY structure. Furthermore, it is important to note that for most of the $X^- + CH_3Y$ systems, except for X = F and Y = Cl, Br, I, the C_{3v} ion-dipole complex is the major,

DOI: 10.1021/acs.jpca.7b11927
J. Phys. Chem. A 2018, 122, 1886−1895

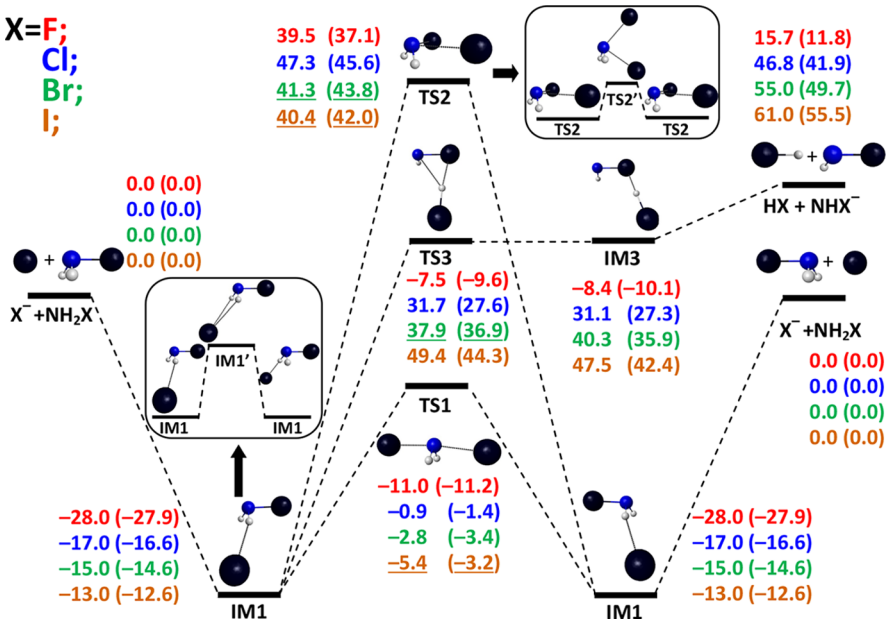

Figure 1. Relative energies (kcal/mol) of stationary points for the $X^- + NH_2X$ [X = F, Cl, Br, I] reactions. The classical energies are obtained at CCSD(T)-F12b/aug-cc-pV5Z(-PP) level of theory at CCSD(T)-F12b/aug-cc-pVTZ(-PP) geometries with core correlation effects obtained as differences between all-electron and frozen-core energies at the CCSD(T)/aug-cc-pwCVTZ(-PP) level of theory at CCSD(T)-F12b/aug-cc-pVTZ(-PP) geometries. The adiabatic energies (in parentheses) are obtained using the classical energies with harmonic zero-point energy corrections at the CCSD(T)-F12b/aug-cc-pVTZ(-PP) level of theory. Effective core potentials and the corresponding pseudopotential (PP) basis sets are used for Br and I. The underlined energies are obtained using MP2/aug-cc-pVDZ(-PP) geometries and frequencies.

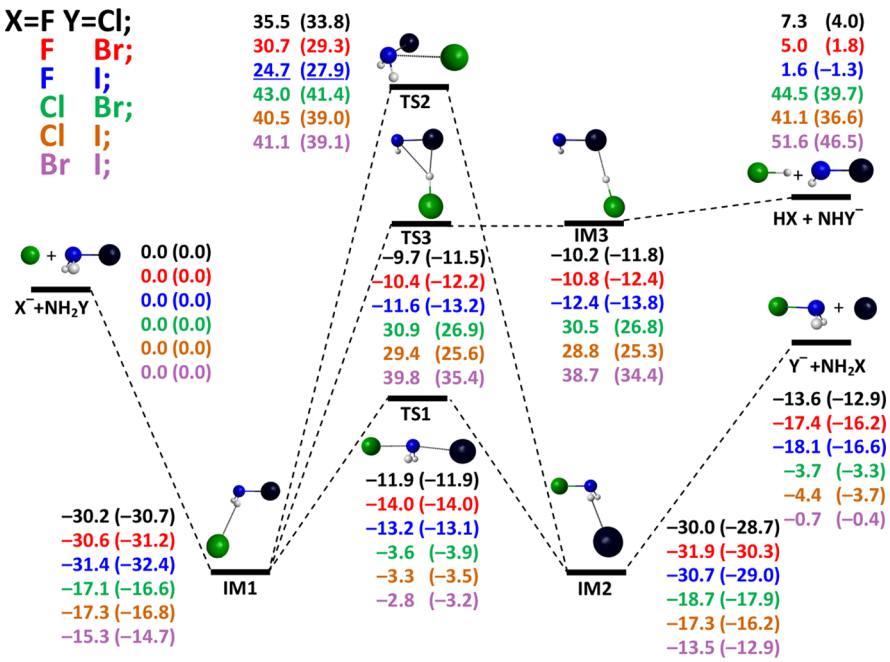

Figure 2. Relative energies (kcal/mol) of stationary points for the $X^- + NH_2Y$ [X,Y = F, Cl, Br, I; X ≠ Y] reactions. The classical energies are obtained at CCSD(T)-F12b/aug-cc-pV5Z(-PP) level of theory at CCSD(T)-F12b/aug-cc-pVTZ(-PP) geometries with core correlation effects obtained as differences between all-electron and frozen-core energies at the CCSD(T)/aug-cc-pwCVTZ(-PP) level of theory at CCSD(T)-F12b/aug-cc-pVTZ(-PP) geometries. The adiabatic energies (in parentheses) are obtained using the classical energies with harmonic zero-point energy corrections at the CCSD(T)-F12b/aug-cc-pVTZ(-PP) level of theory. Effective core potentials and the corresponding pseudopotential (PP) basis sets are used for Br and I. The underlined energies are obtained using MP2/aug-cc-pVDZ(-PP) geometries and frequencies.

deeper minimum, whereas for $X^- + NH_2Y$ the prereaction complex is always H-bonded. For the identity $X^- + NH_2X$ reactions the PES is obviously a symmetry double well; thus, the prereaction and postreaction complexes have the same structure, i.e., IM1 = IM2. For the nonidentity reactions the IM2 complexes, where the leaving group forms a H-bond and the two minima are connected by IM2′ via a negligible barrier, have very similar energies relative to the reactants than IM1, thus, these systems feature nearly symmetric double-well PESs (see Figure 2). This is in sharp contrast to the corresponding C-centered S_N2 reactions, where the postreaction complex is usually the deep global minimum of the PES, especially for X = F, if the atomic number

DOI: 10.1021/acs.jpca.7b11927
J. Phys. Chem. A 2018, 122, 1886−1895

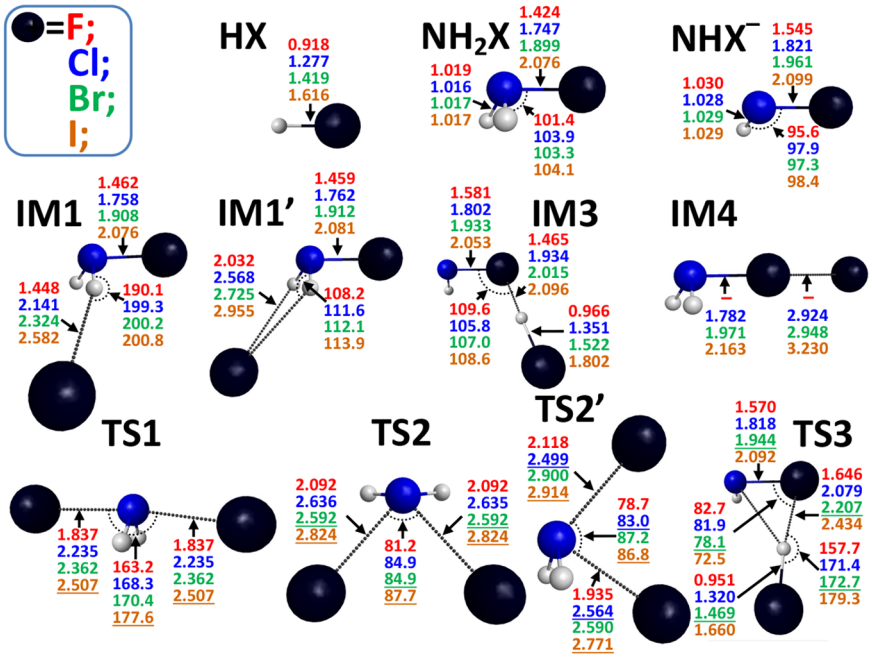

Figure 3. Structures of the stationary points of the X^- + NH_2X [X = F, Cl, Br, I] reactions showing the most important bond lengths (Å) and angles (deg) obtained at the CCSD(T)-F12b/aug-cc-pVTZ-(PP) level of theory. The underlined structural parameters are obtained at the MP2/aug-cc-pVDZ-(PP) level of theory.

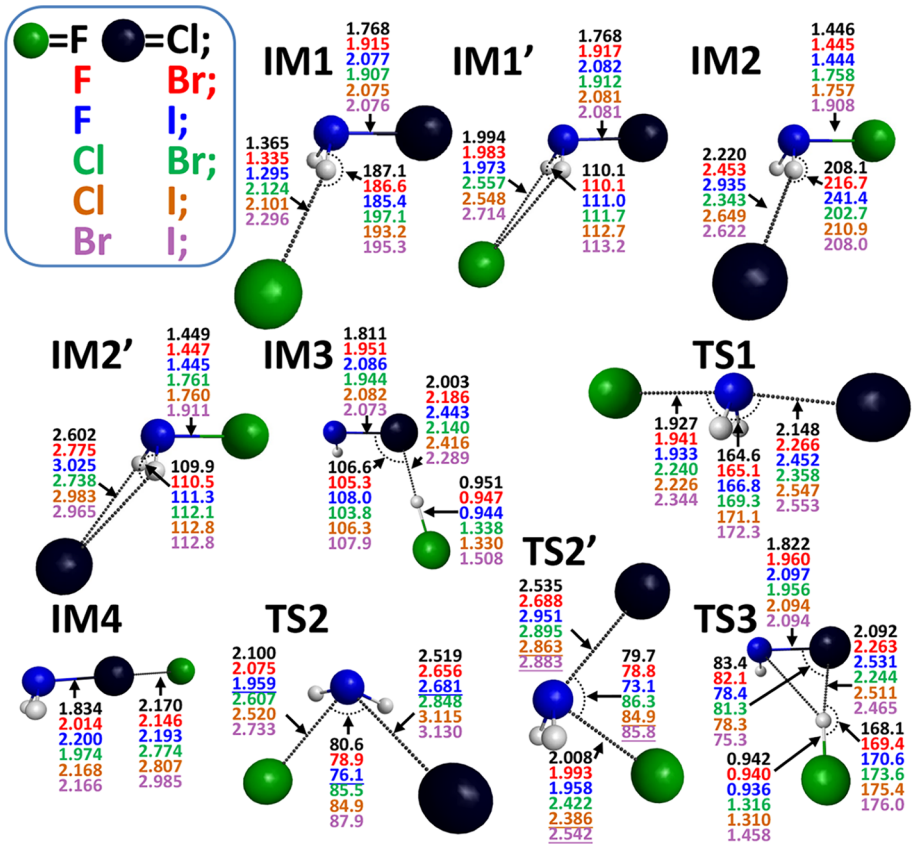

Figure 4. Structures of the stationary points of the X^- + NH_2Y [X,Y = F, Cl, Br, I; X ≠ Y] reactions showing the most important bond lengths (Å) and angles (degrees) obtained at the CCSD(T)-F12b/aug-cc-pVTZ-(PP) level of theory. The underlined structural parameters are obtained at the MP2/aug-cc-pVDZ-(PP) level of theory.

of X is less than Y (X < Y). These findings are in accord with the reaction enthalpies, because the X^- + CH_3Y (X < Y) S_N2 reactions are significantly more exothermic than the corresponding X^- + NH_2Y reaction. For both reaction families the exothermicity increases with increasing Y and decreasing X; thus, the F^- + NH_2I and F^- + CH_3I S_N2 reactions are the most

DOI: 10.1021/acs.jpca.7b11927
J. Phys. Chem. A 2018, 122, 1886−1895

Table 1. Benchmark Classical and Adiabatic Relative Energies, in kcal/mol, Obtained as CCSD(T)-F12b/aug-cc-pV5Z(-PP) + Core Electron Correlation Correction (Δ_{core}) + Zero-Point Energy Correction for the Latter (Δ_{ZPE}) of the Various Minima, Transition States, and Product Channels for the X^- + NH_2X [X = F, Cl, Br, I] Reactions (See Figures 1 and 3 for the Notations)

	5Z[a]	Δ_{core}[b]	Δ_{ZPE}[c]	classical[d]	adiabatic[e]		5Z[a]	Δ_{core}[b]	Δ_{ZPE}[c]	classical[d]	adiabatic[e]
F^- + NH_2F	0.00	0.00	0.00	0.00	0.00	Cl^- + NH_2Cl	0.00	0.00	0.00	0.00	0.00
HF + NHF^-	15.50	0.17	−3.85	15.67	11.82	HCl + $NHCl^-$	46.72	0.12	−4.99	46.84	41.85
H^- + NHF_2	90.83	0.27	−4.99	91.10	86.11	H^- + $NHCl_2$	115.64	−0.02	−5.93	115.62	109.70
F_2 + NH_2^-	97.22	0.24	−4.36	97.45	93.09	Cl_2 + NH_2^-	73.16	0.02	−4.12	73.19	69.06
F_2^- + NH_2	45.51	0.13	−4.72	45.64	40.92	Cl_2^- + NH_2	35.01	0.18	−4.22	35.19	30.97
FHF^- + NH	29.92	0.51	−6.13	30.42	24.29	$ClHCl^-$ + NH	76.55	0.58	−8.44	77.12	68.69
IM1	−27.94	−0.01	0.05	−27.95	−27.89	IM1	−16.97	−0.06	0.45	−17.03	−16.58
IM1′	−23.28	0.00	0.32	−23.28	−22.96	IM1′	−16.02	−0.03	0.27	−16.06	−15.79
IM3	−8.54	0.15	−1.74	−8.39	−10.12	IM3	31.07	0.01	−3.79	31.08	27.29
IM4						IM4	−4.10	−0.03	0.21	−4.13	−3.92
TS1	−11.26	0.28	−0.25	−10.98	−11.23	TS1	−1.19	0.30	−0.48	−0.88	−1.36
TS2	39.27	0.26	−2.43	39.53	37.10	TS2	46.86	0.40	−1.63	47.25	45.62
TS2′	47.47	0.31	−1.88	47.77	45.89	TS2′	48.18[f]	0.48[f]	−1.39[f]	48.66[f]	47.27[f]
TS3	−7.65	0.14	−2.07	−7.51	−9.58	TS3	31.66	0.03	−4.07	31.69	27.62
	5Z[a]	Δ_{core}[b]	Δ_{ZPE}[c]	classical[d]	adiabatic[e]		5Z[a]	Δ_{core}[b]	Δ_{ZPE}[c]	classical[d]	adiabatic[e]
Br^- + NH_2Br	0.00	0.00	0.00	0.00	0.00	I^- + NH_2I	0.00	0.00	0.00	0.00	0.00
HBr + $NHBr^-$	54.95	0.01	−5.29	54.96	49.67	HI + NHI^-	61.12	−0.10	−5.53	61.02	55.50
H^- + NHF_2	119.59	−0.18	−6.24	119.41	113.17	H^- + NHI_2	120.83	−0.39	−6.41	120.44	114.03
Br_2 + NH_2^-	69.62	0.06	−4.08	69.68	65.60	I_2 + NH_2^-	65.82	0.10	−3.91	65.92	62.01
Br_2^- + NH_2	27.96	0.14	−3.99	28.10	24.11	I_2^- + NH_2	24.60	0.11	−3.73	24.71	20.98
$BrHBr^-$ + NH	86.08	0.15	−8.35	86.23	77.88	IHI^- + NH	99.31	−0.24	−8.52	99.08	90.55
IM1	−14.84	−0.19	0.43	−15.03	−14.60	IM1	−12.59	−0.41	0.42	−12.99	−12.58
IM1′	−14.31	−0.16	0.21	−14.47	−14.26	IM1′	−12.30	−0.35	0.19	−12.64	−12.45
IM3	40.52	−0.27	−4.40	40.25	35.85	IM3	48.20	−0.67	−5.14	47.53	42.40
IM4	−9.39	−0.13	0.00	−9.52	−9.52	IM4	−13.63	−0.33	−0.08	−13.96	−14.04
TS1	−2.92	0.10	−0.53	−2.82	−3.35	TS1	−5.05[f]	−0.39[f]	2.26[f]	−5.44[f]	−3.18[f]
TS2	41.15[f]	0.12[f]	2.49[f]	41.27[f]	43.76[f]	TS2	40.56[f]	−0.18[f]	1.60[f]	40.37[f]	41.97[f]
TS2′	44.98	0.35	−2.08	45.33	43.25	TS2′	37.24[f]	0.79[f]	0.39[f]	38.03[f]	38.42[f]
TS3	38.26[f]	−0.33[f]	−1.05[f]	37.93[f]	36.89[f]	TS3	50.01	−0.64	−5.04	49.37	44.33

[a]Frozen-core energies obtained at the CCSD(T)-F12b/aug-cc-pV5Z(-PP) level of theory at CCSD(T)-F12b/aug-cc-pVTZ(-PP) geometries. [b]Core correlation effects obtained as differences between all-electron and frozen-core energies at the CCSD(T)/aug-cc-pwCVTZ(-PP) level of theory at CCSD(T)-F12b/aug-cc-pVTZ(-PP) geometries. [c]Harmonic zero-point energy corrections at the CCSD(T)-F12b/aug-cc-pVTZ(-PP) level of theory. [d]Benchmark classical relative energies obtained as CCSD(T)-F12b/aug-cc-pV5Z(-PP) + Δ_{core}. [e]Benchmark adiabatic relative energies obtained as CCSD(T)-F12b/aug-cc-pV5Z(-PP) + Δ_{core} + Δ_{ZPE}. [f]These results are obtained using MP2/aug-cc-pVDZ(-PP) geometries.

exothermic with 0 K reaction enthalpies of −16.6 and −45.2[15] kcal/mol, respectively.

Besides the back-side attack H-bonded complexes we have also found halogen-bonded front-side attack minima (IM4, C_s symmetry), where X^- connects to Y (see Figures 3 and 4). The $X^-\cdots YNH_2$ front-side complex is the most stable if Y = I and in these cases the IM4 minima are deeper than the corresponding IM1. For the F^- + NH_2I reaction the front-side IM4 is the global minimum of the PES with classical depth of 35.9 kcal/mol, whereas the corresponding IM1 is 31.4 kcal/mol deep. In the case of smaller leaving groups the front-side complexes are less stable, for example, the $Cl^-\cdots ClNH_2$ minimum is only 4.1 kcal/mol deep, whereas the depth of the H-bonded IM1 is 17.0 kcal/mol, and we could not find a front-side minimum for the F^- + NH_2F system. Similar front-side minima were recently reported for the C-centered S_N2 reactions as well.[7,8,15,38,39] As the H-bonded minima, the front-side minima are deeper for the N-centered reactions than the corresponding C-centered analogue. For the latter, the $F^-\cdots ICH_3$ complex with depth of 22.6 kcal/mol was also found to be more stable than the H-bonded complex with dissociation energy of 20.3 kcal/mol.[15] Our recent dynamics simulations for the F^- + CH_3I reaction revealed significant front-side complex formation;[8] thus, IM4 may play an important role in the mechanisms of some of the N-centered S_N2 reactions as well.

The above-described substitution pathway of the X^- + NH_2Y reactions via the submerged TS1 is the back-side attack Walden-inversion mechanism of N-centered S_N2 reactions. As shown in Figures 1 and 2 there is a front-side attack retention S_N2 pathway via a high barrier corresponding to a transition state denoted by TS2. The barriers are around 40 kcal/mol for X = Cl, Br, I and smaller for X = F. The smallest front-side attack classical barrier of 24.7 kcal/mol is found for the F^- + NH_2I reaction, whereas the corresponding value for F^- + CH_3I is 20.1 kcal/mol,[15] which is also the smallest among the analogous C-centered S_N2 reactions.[40] TS2 of the identity X^- + NH_2X systems has C_s symmetry, where only the N atom is involved in C_s plane as shown in Figure 3. The N−X bonds are stretched by 0.6−0.9 Å relative to the corresponding bond lengths of the NH_2X molecules and the XNX angles are around 85°. In the case of the nonidentity reactions TS2 has similar structure as described above; however, due to the different ligands the C_s symmetry obviously breaks (see Figure 4). In both the identity and nonidentity cases two equivalent TS2s exist corresponding to the exchange of the X, X and X, Y atoms, respectively. In both cases we have found a second-order saddle point (TS2′, C_s symmetry),

DOI: 10.1021/acs.jpca.7b11927
J. Phys. Chem. A 2018, 122, 1886−1895

Table 2. Benchmark Classical and Adiabatic Relative Energies, in kcal/mol, Obtained as CCSD(T)-F12b/aug-cc-pV5Z(-PP) + Core Electron Correlation Correction (Δ_{core}) + Zero-Point Energy Correction for the Latter (Δ_{ZPE}) of the various Minima, Transition States, and Product Channels for the X^- + NH_2Y [X,Y = F, Cl, Br, I] Nonidentity Reactions (See Figures 2 and 4 for the Notations)

	5Z[a]	Δ_{core}[b]	Δ_{ZPE}[c]	classical[d]	adiabatic[e]		5Z[a]	Δ_{core}[b]	Δ_{ZPE}[c]	classical[d]	adiabatic[e]
F^- + NH_2Cl	0.00	0.00	0.00	0.00	0.00	F^- + NH_2Br	0.00	0.00	0.00	0.00	0.00
Cl^- + NH_2F	−13.90	0.27	0.77	−13.64	−12.87	Br^- + NH_2F	−17.68	0.33	1.14	−17.35	−16.21
HF + $NHCl^-$	7.07	0.24	−3.35	7.31	3.96	HF + $NHBr^-$	4.62	0.35	−3.15	4.97	1.82
H^- + NHClF	98.09	0.27	−5.16	98.36	93.20	H^- + NHBrF	99.12	0.20	−5.17	99.32	94.15
ClF + NH_2^-	64.61	0.22	−3.79	64.83	61.04	BrF + NH_2^-	56.34	0.58	−3.58	56.91	53.33
ClF^- + NH_2	30.52	0.28	−4.07	30.81	26.74	BrF^- + NH_2	21.88	0.42	−3.77	22.30	18.54
$ClHF^-$+ NH	36.80	0.73	−4.50	37.52	33.02	$BrHF^-$ + NH	36.44	0.66	−4.20	37.10	32.90
IM1	−30.24	0.02	−0.45	−30.22	−30.67	IM1	−30.64	0.04	−0.61	−30.60	−31.21
IM1′	−23.72	0.02	0.40	−23.70	−23.30	IM1′	−23.69	0.02	0.32	−23.67	−23.35
IM2	−30.17	0.20	1.28	−29.96	−28.69	IM2	−32.04	0.17	1.57	−31.87	−30.31
IM2′	−29.81	0.22	1.04	−29.59	−28.55	IM2′	−31.98	0.19	1.36	−31.80	−30.44
IM3	−10.35	0.15	−1.56	−10.20	−11.76	IM3	−10.99	0.17	−1.53	−10.82	−12.35
IM4	−12.13	0.06	0.30	−12.06	−11.77	IM4	−23.60	0.22	0.25	−23.38	−23.13
TS1	−12.26	0.41	−0.08	−11.85	−11.93	TS1	−14.32	0.32	0.04	−13.99	−13.96
TS2	35.01	0.46	−1.72	35.47	33.75	TS2	30.09	0.61	−1.43	30.70	29.27
TS2′	38.02	0.52	−1.34	38.54	37.20	TS2′	31.99	0.71	−1.37	32.70	31.33
TS3	−9.87	0.16	−1.83	−9.71	−11.54	TS3	−10.52	0.16	−1.79	−10.36	−12.15
	5Z[a]	Δ_{core}[b]	Δ_{ZPE}[c]	classical[d]	adiabatic[e]		5Z[a]	Δ_{core}[b]	Δ_{ZPE}[c]	classical[d]	adiabatic[e]
F^- + NH_2I	0.00	0.00	0.00	0.00	0.00	Cl^- + NH_2Br	0.00	0.00	0.00	0.00	0.00
I^- + NH_2F	−18.53	0.48	1.46	−18.05	−16.59	Br^- + NH_2Cl	−3.78	0.07	0.37	−3.71	−3.34
HF + NHI^-	1.23	0.37	−2.92	1.60	−1.32	HCl + $NHBr^-$	44.27	0.23	−4.80	44.50	39.70
H^- + NHIF	100.83	0.16	−5.16	100.99	95.82	H^- + NHBrCl	115.77	−0.07	−5.90	115.70	109.80
IF + NH_2^-	44.62	1.06	−3.33	45.68	42.36	BrCl + NH_2^-	69.28	0.14	−3.91	69.42	65.50
IF^- + NH_2	14.07	0.73	−3.46	14.81	11.35	$BrCl^-$ + NH_2	29.18	0.22	−3.91	29.40	25.48
IHF^- + NH	39.24	0.67	−3.95	39.91	35.96	$BrHCl^-$ + NH	77.43	0.49	−6.79	77.92	71.13
IM1	−31.40	−0.01	−0.95	−31.41	−32.36	IM1	−16.99	−0.07	0.47	−17.06	−16.59
IM1′	−23.58	−0.05	0.34	−23.63	−23.30	IM1′	−15.91	−0.05	0.29	−15.96	−15.67
IM2	−30.91	0.22	1.68	−30.68	−29.00	IM2	−18.62	−0.11	0.79	−18.73	−17.94
IM2′	−30.92	0.22	1.74	−30.69	−28.96	IM2′	−18.19	−0.08	0.58	−18.26	−17.69
IM3	−12.49	0.10	−1.42	−12.39	−13.81	IM3	30.45	0.03	−3.71	30.47	26.76
IM4	−36.39	0.52	0.27	−35.86	−35.59	IM4	−11.10	0.00	0.09	−11.10	−11.01
TS1	−13.45	0.21	0.15	−13.24	−13.09	TS1	−3.82	0.23	−0.33	−3.60	−3.92
TS2	24.18[f]	0.53[f]	3.22[f]	24.71[f]	27.93[f]	TS2	42.40	0.59	−1.56	42.98	41.42
TS2′	27.95	0.96	−1.17	28.91	27.74	TS2′	44.60	0.53	−1.57	45.13	43.56
TS3	−11.65	0.07	−1.61	−11.58	−13.19	TS3	30.84	0.03	−3.97	30.87	26.90
	5Z[a]	Δ_{core}[b]	Δ_{ZPE}[c]	classical[d]	adiabatic[e]		5Z[a]	Δ_{core}[b]	Δ_{ZPE}[c]	classical[d]	adiabatic[e]
Cl^- + NH_2I	0.00	0.00	0.00	0.00	0.00	Br^- + NH_2I	0.00	0.00	0.00	0.00	0.00
I^- + NH_2Cl	−4.63	0.22	0.69	−4.41	−3.72	I^- + NH_2Br	−0.85	0.15	0.32	−0.70	−0.38
HCl + NHI^-	40.87	0.26	−4.56	41.12	36.56	HBr + NHI^-	51.55	0.04	−5.06	51.59	46.53
H^- + NHICl	116.33	−0.11	−5.84	116.21	110.38	H^- + NHIBr	119.94	−0.21	−6.18	119.73	113.55
ICl + NH_2^-	64.30	0.43	−3.67	64.73	61.06	IBr + NH_2^-	66.11	0.22	−3.83	66.33	62.50
ICl^- + NH_2	25.28	0.41	−3.62	25.69	22.07	IBr^- + NH_2	25.16	0.26	−3.70	25.42	21.72
$IHCl^-$ + NH	80.66	0.48	−6.25	81.14	74.89	$IHBr^-$ + NH	90.65	0.12	−7.19	90.77	83.58
IM1	−17.20	−0.12	0.53	−17.32	−16.79	IM1	−14.99	−0.26	0.52	−15.25	−14.73
IM1′	−15.75	−0.11	0.30	−15.86	−15.56	IM1′	−14.17	−0.22	0.23	−14.40	−14.16
IM2	−17.17	−0.10	1.05	−17.26	−16.21	IM2	−13.35	−0.18	0.66	−13.54	−12.88
IM2′	−17.11	−0.05	0.85	−17.16	−16.30	IM2′	−13.25	−0.14	0.50	−13.39	−12.89
IM3	28.91	−0.07	−3.55	28.84	25.29	IM3	39.10	−0.39	−4.29	38.70	34.41
IM4	−19.01	0.09	0.07	−18.92	−18.85	IM4	−16.45	−0.10	−0.03	−16.55	−16.58
TS1	−3.45	0.12	−0.18	−3.32	−3.50	TS1	−2.83	0.01	−0.38	−2.82	−3.20
TS2	39.78	0.71	−1.50	40.49	38.98	TS2	40.48	0.64	−2.00	41.13	39.13
TS2′	31.51[f]	2.82[f]	5.78[f]	34.32[f]	40.11[f]	TS2′	35.70[f]	2.20[f]	5.62[f]	37.90[f]	43.52[f]
TS3	29.52	−0.08	−3.80	29.44	25.64	TS3	40.21	−0.38	−4.42	39.82	35.40

[a]Frozen-core energies obtained at the CCSD(T)-F12b/aug-cc-pV5Z(-PP) level of theory at CCSD(T)-F12b/aug-cc-pVTZ(-PP) geometries. [b]Core correlation effects obtained as differences between all-electron and frozen-core energies at the CCSD(T)/aug-cc-pwCVTZ(-PP) level of theory at CCSD(T)-F12b/aug-cc-pVTZ(-PP) geometries. [c]Harmonic zero-point energy corrections at the CCSD(T)-F12b/aug-cc-pVTZ(-PP) level of

DOI: 10.1021/acs.jpca.7b11927
J. Phys. Chem. A 2018, 122, 1886−1895

Table 2. continued

theory. [d]Benchmark classical relative energies obtained as CCSD(T)-F12b/aug-cc-pV5Z(-PP) + Δ_{core}. [e]Benchmark adiabatic relative energies obtained as CCSD(T)-F12b/aug-cc-pV5Z(-PP) + Δ_{core} + Δ_{ZPE}. [f]These results are obtained using MP2/aug-cc-pVDZ(-PP) geometries.

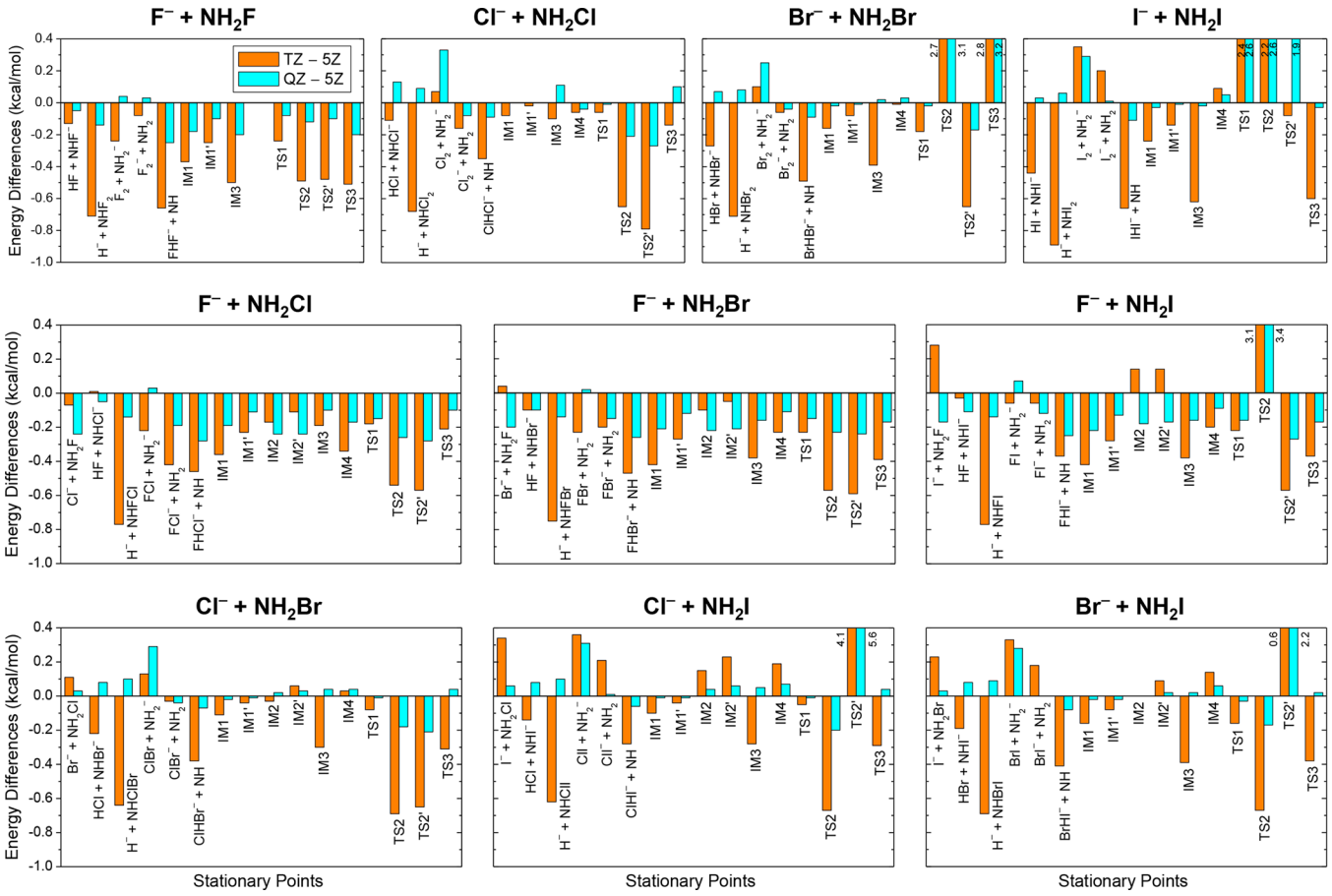

Figure 5. Convergence of the CCSD(T)-F12b relative energies for the product channels and stationary points of the $X^- + NH_2Y$ [X,Y = F, Cl, Br, I] reactions using the aug-cc-pVTZ(-PP), aug-cc-pVQZ(-PP), and aug-cc-pV5Z(-PP) basis sets.

where N, X, X and N, X, Y atoms are in the C_s plane, connecting the two equivalent TS2 first-order stationary points as seen in Figure 1. The classical barrier between the two TS2 is the highest for $F^- + NH_2F$, 8.2 kcal/mol, and becomes almost negligible for the heavier ligands. Similar front-side attack transition-state structures were previously reported for the $X^- + CH_3Y$ reactions; however, for the C-centered reactions the first-order saddle points are TS2′-like for X = F and Y = F, Cl, Br, I (C_s symmetry with C, H, X, Y in one plane) and TS2-like for the other cases.[40]

As shown in Figures 1 and 2 proton transfer can also occur between X^- and NH_2Y resulting in HX + NHY^- products. Proton transfer is highly endothermic for X = Cl, Br, I with reaction enthalpies around 40−50 kcal/mol, whereas for X = F the 0 K reaction enthalpies are only 11.8, 4.0, 1.8, and −1.3 kcal/mol for Y = F, Cl, Br, and I, respectively. The $F^- + NH_2I \rightarrow HF + NHI^-$ reaction is nearly isoenergetic and the ZPE correction changes the sign of the reaction enthalpy from +1.6 to −1.3 kcal/mol. A transition state (TS3) and a minimum (IM3) have been found in the proton transfer region; both can be consider as postreaction stationary points, where the N···H bond is nearly broken and the H−X distance is stretched by only 0.05−0.2 Å relative to the corresponding bond length in the HX molecule. Similar to the $X^- + CH_3Y$ systems, all the TS3 and IM3 stationary points are below the corresponding product asymptotes; thus, energetically proton transfer can occur if enough energy is available to overcome the endothermicity. Note that in the proton-transfer region additional stationary points may exist as many of them were found recently for the $F^- + CH_3I$ and $Cl^- + CH_3I$ reactions.[41,15,17]

Besides the above-discussed S_N2 ($Y^- + NH_2X$) and proton-transfer (HX + NHY^-) channels, we have also investigated additional endothermic product channels of the $X^- + NH_2Y$ [X,Y = F, Cl, Br, I] reactions such as H^- + NHXY, XY^- + NH_2, XY + NH_2^-, and XHY^- + NH as shown in Tables 1 and 2. Hydride substitution leading to H^- + NHXY is highly endothermic since the binding energy of the forming N−X bond is significantly less than that of an N−H bond. The reaction enthalpies are around 90−120 kcal/mol and the ZPE corrections decrease them by 5−7 kcal/mol. Halogen abstraction is more endothermic than proton abstraction as the 0 K reaction enthalpies of the former are usually in the range of 20−30 kcal/mol with the extremes of 11.3 and 40.9 kcal/mol for $F^- + NH_2I$ and $F^- + NH_2F$, respectively. Halogen abstraction forms two doublet products, XY^- and NH_2, which can occur on a singlet PES. We have investigated the XY + NH_2^- channel of two singlet products, but, as Tables 1 and 2 show, this channel is higher in energy by 30−55 kcal/mol than the corresponding XY^- + NH_2; thus, on the ground-state singlet PES the XY^- + NH_2 products can be formed.

DOI: 10.1021/acs.jpca.7b11927
J. Phys. Chem. A 2018, 122, 1886−1895

Another possible product channel is XHY^- + NH, which is more endothermic than XY^- + NH_2, except for F^- + NH_2F, where the 0 K reaction enthalpy of FHF^- + NH is only 24.3 kcal/mol. For X = F and Y = F, Cl, Br, I the reaction enthalpies are in the 24−36 kcal/mol range, whereas for X, Y = Cl, Br, I, the reaction enthalpies are in a higher range of 68−91 kcal/mol as shown in Tables 1 and 2.

On the basis of the detailed electronic structure data, we can analyze the accuracy of our benchmark predictions for the energetics of the title reactions. Figure 5 shows the convergence of the CCSD(T)-F12b relative energies with respect to the size of the basis set for all the stationary points presented in Tables 1 and 2. Usually a smooth convergence is seen when increasing the basis as aug-cc-pVTZ(-PP) (TZ) → aug-cc-pVQZ(-PP) (QZ) → aug-cc-pV5Z(-PP) (5Z). The TZ and 5Z data agree within 0.2−0.8 kcal/mol and the accuracy of the QZ results is often better than 0.2 kcal/mol. For the most important stationary points, such as the S_N2 product channel (Y^- + NH_2X), Walden-inversion transition state (TS1), and pre- (IM1) and postreaction (IM2) complexes, the TZ and QZ bases usually converge within 0.3 and 0.1 kcal/mol, respectively. In a few cases, especially for the high-energy front-side attack transition states (TS2 and TS2′) with Br and/or I, the 5Z relative energies substantially differ from the TZ and QZ data as shown in Figure 5. For all these outliers the CCSD(T)-F12b geometry optimizations do not converge and the energy computations are performed at MP2 structures. Furthermore, T_1 diagnostics[42] show that TS2 and TS2′ have strong multireference character, because the T_1 values are as large as 0.04−0.10. Nevertheless, for the other stationary points the T_1 values are well below 0.02 or only slightly above for TS1; thus, in these cases the use of the single-reference methods is adequate. As Tables 1 and 2 show the core electron correlation effects are usually small, but comparable with the basis set error. Furthermore, in some cases, especially for TS2 and TS2′, the core correlation contribution can be larger than 0.5 kcal/mol; thus, not negligible if we aim for subchemical accuracy. Post-CCSD(T) correlation effects are not considered in this study; nevertheless, they are usually small, i.e., a few tenths of kcal/mol.[43,17] Of course, for TS2 and TS2′ where the T_1 values are large, one may expect much substantial post-CCSD(T) correlation contributions. The ZPE corrections are often large, especially for the different product channels, where Δ_{ZPE} can be around −4 kcal/mol, as seen in Tables 1 and 2. Furthermore, the proton-transfer product-like TS3 and IM3 have also large ZPE corrections of around −4 kcal/mol, in accord with the Δ_{ZPE} of the corresponding HX + NHY^- product channels. On the basis of the above discussion, we can conclude that the present benchmark relative energies are accurate within a few tenths of kcal/mol, although the TS2/TS2′ data and some of the adiabatic results may have somewhat larger uncertainties due to the multireference character and the neglected anharmonicity of the vibrational frequencies, respectively.

IV. SUMMARY AND CONCLUSIONS

Motivated by the recent studies on C-centered S_N2 reactions revealing several novel stationary points playing important roles in the dynamics,[10,11] we have characterized the PESs of the X^- + NH_2Y [X,Y = F, Cl, Br, I] systems using high-level explicitly correlated coupled cluster computations. Besides several stationary points for the S_N2 and proton-transfer processes, we have determined the reaction enthalpies of various endothermic product channels. Unlike many previous DFT and MP2 studies, we have performed geometry optimizations and harmonic frequency computations using the CCSD(T)-F12b/aug-cc-pVTZ-(-PP) level of theory with relativistic effective core potentials for Br and I. The best, benchmark-quality relative energies are obtained at the above-defined geometries with the CCSD(T)-F12b/aug-cc-pV5Z(-PP) level of theory considering additive core correlation and ZPE corrections, thereby usually achieving an accuracy within a few tenths of kcal/mol.

In the entrance and exit channels of all the X^- + NH_2Y S_N2 reactions there are deep H-bonded pre- and postreaction minima (C_1 symmetry) separated by a first-order submerged Walden-inversion transition state. The two equivalent H-bonded C_1 minima are connected via a first-order saddle point of C_s symmetry. Motivated by our previous work on the F^- + CH_3Y [Y = Cl and I] reactions,[7,8] we have also found halogen-bonded front-side complexes, which are more stable than the corresponding H-bonded complexes for Y = I. Besides the back-side attack Walden-inversion pathway a high-energy front-side attack mechanism also exists via transition state of C_s and C_1 symmetry for the identity and nonidentity systems, respectively. The two equivalent front-side attack TSs corresponding to halogen exchange are connected via a second-order saddle point of C_s symmetry, where XNY is in the C_s plane. Proton transfer, which is a low-energy product channel for F^- nucleophile, proceeds through product-like stationary points with energies below the product asymptote. We report a transition state and a minimum for the proton-transfer region, but based on similar studies on C-centered reactions, additional stationary points can be expected. Among the other endothermic product channels the halogen abstraction (XY^- + NH_2) and XHY^- + NH formation are found to be the most important, that may play a role at accessible collision energies.

To gain more insight into the dynamics and mechanisms of the X^- + NH_2Y reactions, dynamics simulations would be desired. Such simulations could investigate the effects of (a) the nucleophile, (b) the leaving group, (c) the central atom in comparison to C-centered reactions, (d) H-bonded complex formation, (e) front-side complex formation, as well as the competition between (f) direct and indirect dynamics, (g) inversion and retention, (h) S_N2, proton-transfer, and other high-energy product channels, etc. Furthermore, these dynamics computations may reveal double inversion[6] in N-centered S_N2 reactions, which was not investigated in this study, because double inversion may be a nonintrinsic−reaction−coordinate pathway.[44] A simulation was recently performed for the F^- + NH_2Cl reaction using the direct dynamics method.[28] In the near future we plan to apply an analytical ab initio PES-based approach to perform efficient trajectory computations for an X^- + NH_2Y reaction. For the analytical PES development the present high-level ab initio study provides definitive guidance since knowing the stationary points and energetically available product channels is necessary. Furthermore, the present work may motivate further theoretical and experimental investigations of N-centered S_N2 reaction, which would be desired, because the dynamics of N-centered S_N2 reactions is "largely unclear" compared to the well-studied C-centered systems as Liu et al.[28] concluded recently.

■ ASSOCIATED CONTENT

Supporting Information

The Supporting Information is available free of charge on the ACS Publications website at DOI: 10.1021/acs.jpca.7b11927.

Structures, energies, and vibrational frequencies of all the stationary points considered in this study at different ab initio levels of theory (PDF)

DOI: 10.1021/acs.jpca.7b11927
J. Phys. Chem. A 2018, 122, 1886−1895

AUTHOR INFORMATION

Corresponding Author

*(G.C.) E-mail: gczako@chem.u-szeged.hu.

ORCID

Gábor Czakó: 0000-0001-5136-4777

Notes

The authors declare no competing financial interest.

ACKNOWLEDGMENTS

G.C. thanks the Scientific Research Fund of Hungary (PD-111900 and K-125317) for financial support. We acknowledge the National Information Infrastructure Development Institute for awarding us access to resources based in Hungary at Szeged and Debrecen.

REFERENCES

(1) Walden, P. Ueber die Gegenseitige Umwandlung Optischer Antipoden. *Ber. Dtsch. Chem. Ges.* **1896**, *29*, 133−138.

(2) Cowdrey, W. A.; Hughes, E. D.; Ingold, C. K.; Masterman, S.; Scott, A. D. Reaction Kinetics and the Walden Inversion. Part VI. Relation of Steric Orientation to Mechanism in Substitutions Involving Halogen Atoms and Simple or Substituted Hydroxyl Groups. *J. Chem. Soc.* **1937**, *1937*, 1252−1271.

(3) Sun, L.; Song, K.; Hase, W. L. A S_N2 Reaction That Avoids Its Deep Potential Energy Minimum. *Science* **2002**, *296*, 875−878.

(4) Gonzales, J. M.; Pak, C.; Cox, R. S.; Allen, W. D.; Schaefer, H. F., III; Császár, A. G.; Tarczay, G. Definitive ab Initio Studies of Model S_N2 Reactions $CH_3X + F^-$ (X = F, Cl, CN, OH, SH, NH_2, PH_2). *Chem. - Eur. J.* **2003**, *9*, 2173−2192.

(5) Mikosch, J.; Trippel, S.; Eichhorn, C.; Otto, R.; Lourderaj, U.; Zhang, J.-X.; Hase, W. L.; Weidemüller, M.; Wester, R. Imaging Nucleophilic Substitution Dynamics. *Science* **2008**, *319*, 183−186.

(6) Szabó, I.; Czakó, G. Revealing a Double-Inversion Mechanism for the $F^- + CH_3Cl$ S_N2 Reaction. *Nat. Commun.* **2015**, *6*, 5972.

(7) Stei, M.; Carrascosa, E.; Kainz, M. A.; Kelkar, A. H.; Meyer, J.; Szabó, I.; Czakó, G.; Wester, R. Influence of the Leaving Group on the Dynamics of a Gas-Phase S_N2 Reaction. *Nat. Chem.* **2016**, *8*, 151−156.

(8) Szabó, I.; Olasz, B.; Czakó, G. Deciphering Front-Side Complex Formation in S_N2 Reactions via Dynamics Mapping. *J. Phys. Chem. Lett.* **2017**, *8*, 2917−2923.

(9) Xie, J.; Otto, R.; Mikosch, J.; Zhang, J.; Wester, R.; Hase, W. L. Identification of Atomic-Level Mechanisms for Gas-Phase $X^- + CH_3Y$ S_N2 Reactions by Combined Experiments and Simulations. *Acc. Chem. Res.* **2014**, *47*, 2960−2969.

(10) Xie, J.; Hase, W. L. Rethinking the S_N2 Reaction. *Science* **2016**, *352*, 32−33.

(11) Szabó, I.; Czakó, G. Dynamics and Novel Mechanisms of S_N2 Reactions on ab Initio Analytical Potential Energy Surfaces. *J. Phys. Chem. A* **2017**, *121*, 9005−9019.

(12) Mikosch, J.; Zhang, J.; Trippel, S.; Eichhorn, C.; Otto, R.; Sun, R.; de Jong, W. A.; Weidemüller, M.; Hase, W. L.; Wester, R. Indirect Dynamics in a Highly Exoergic Substitution Reaction. *J. Am. Chem. Soc.* **2013**, *135*, 4250−4259.

(13) Szabó, I.; Császár, A. G.; Czakó, G. Dynamics of the $F^- + CH_3Cl \rightarrow Cl^- + CH_3F$ S_N2 Reaction on a Chemically Accurate Potential Energy Surface. *Chem. Sci.* **2013**, *4*, 4362−4370.

(14) Szabó, I.; Telekes, H.; Czakó, G. Accurate ab Initio Potential Energy Surface, Thermochemistry, and Dynamics of the $F^- + CH_3F$ S_N2 and Proton-Abstraction Reactions. *J. Chem. Phys.* **2015**, *142*, 244301.

(15) Olasz, B.; Szabó, I.; Czakó, G. High-Level ab Initio Potential Energy Surface and Dynamics of the $F^- + CH_3I$ S_N2 and Proton-Transfer Reactions. *Chem. Sci.* **2017**, *8*, 3164−3170.

(16) Tajti, V.; Czakó, G. Benchmark ab Initio Characterization of the Complex Potential Energy Surface of the $F^- + CH_3CH_2Cl$ Reaction. *J. Phys. Chem. A* **2017**, *121*, 2847−2854.

(17) Szabó, I.; Czakó, G. Benchmark ab Initio Characterization of the Complex Potential Energy Surface of the $Cl^- + CH_3I$ Reaction. *J. Phys. Chem. A* **2017**, *121*, 5748−5757.

(18) Bühl, M.; Schaefer, H. F., III S_N2 Reaction at Neutral Nitrogen: Transition State Geometries and Intrinsic Barriers. *J. Am. Chem. Soc.* **1993**, *115*, 9143−9147.

(19) Glukhovtsev, M. N.; Pross, A.; Radom, L. Gas-Phase Identity S_N2 Reactions of Halide Ions at Neutral Nitrogen: A High-Level Computational Study. *J. Am. Chem. Soc.* **1995**, *117*, 9012−9018.

(20) Gareyev, R.; Kato, S.; Bierbaum, V. M. Gas Phase Reactions of NH_2Cl with Anionic Nucleophiles: Nucleophilic Substitution at Neutral Nitrogen. *J. Am. Soc. Mass Spectrom.* **2001**, *12*, 139−143.

(21) Yang, J.; Ren, Y.; Zhu, H.; Chu, S.-Y. Gas-Phase Non-Identity S_N2 Reactions at Neutral Nitrogen: a Hybrid DFT Study. *Int. J. Mass Spectrom.* **2003**, *229*, 199−208.

(22) Ren, Y.; Zhu, H. A G2(+) Level Investigation of the Gas-Phase Non-Identity S_N2 Reactions of Halides with Halodimethylamine. *J. Am. Soc. Mass Spectrom.* **2004**, *15*, 673−680.

(23) Xing, Y.-M.; Xu, X.-F.; Cai, Z.-S.; Zhao, X.-Z. DFT Study on the Behavior and Reactivity of Electron Transfer in Gas-Phase Symmetric $X_a^- + NH_2X_b \rightarrow X_aNH_2 + X_b^-$ (X = F,Cl,Br and I) Reactions. *J. Mol. Struct.: THEOCHEM* **2004**, *671*, 27−37.

(24) Yu, F.; Song, L.; Zhou, X. Ab Initio Molecular Dynamics Investigations on the S_N2 Reactions of OH^- with NH_2F and NH_2Cl. *Comput. Theor. Chem.* **2011**, *977*, 86−91.

(25) Yu, F. Ab Initio Direct Classical Trajectory Investigation on the S_N2 Reaction of F^- with NH_2F: Nonstatistical Central Barrier Recrossing Dynamics. *J. Comput. Chem.* **2012**, *33*, 401−405.

(26) Lv, J.; Zhang, J.; Wang, D. A Multi-Level Quantum Mechanics and Molecular Mechanics Study of S_N2 Reaction at Nitrogen: $NH_2Cl + OH^-$ in Aqueous Solution. *Phys. Chem. Chem. Phys.* **2016**, *18*, 6146−6152.

(27) Liu, X.; Zhang, J.; Yang, L.; Sun, R. Theoretical Studies on $F^- + NH_2Cl$ Reaction: Nucleophilic Substitution at Neutral Nitrogen. *J. Phys. Chem. A* **2016**, *120*, 3740−3746.

(28) Liu, X.; Zhao, C.; Yang, L.; Zhang, J.; Sun, R. Indirect Dynamics in S_N2@N: Insight into the Influence of Central Atoms. *Phys. Chem. Chem. Phys.* **2017**, *19*, 22691−22699.

(29) Kubelka, J.; Bickelhaupt, M. F. Activation Strain Analysis of S_N2 Reactions at C, N, O, and F Centers. *J. Phys. Chem. A* **2017**, *121*, 885−891.

(30) Adler, T. B.; Knizia, G.; Werner, H.-J. A Simple and Efficient CCSD(T)-F12 Approximation. *J. Chem. Phys.* **2007**, *127*, 221106.

(31) Dunning, T. H., Jr. Gaussian Basis Sets for Use in Correlated Molecular Calculations. I. The Atoms Boron Through Neon and Hydrogen. *J. Chem. Phys.* **1989**, *90*, 1007−1023.

(32) Peterson, K. A.; Figgen, D.; Goll, E.; Stoll, H.; Dolg, M. Systematically Convergent Basis Sets with Relativistic Pseudopotentials. II. Small-Core Pseudopotentials and Correlation Consistent Basis Sets for the Post-*d* Group 16−18 Elements. *J. Chem. Phys.* **2003**, *119*, 11113−11123.

(33) Møller, C.; Plesset, M. S. Note on an Approximation Treatment for Many-Electron Systems. *Phys. Rev.* **1934**, *46*, 618−622.

(34) Amos, R. D.; Andrews, J. S.; Handy, N. C.; Knowles, P. J. Open-Shell Møller−Plesset Perturbation Theory. *Chem. Phys. Lett.* **1991**, *185*, 256−264.

(35) Knowles, P. J.; Hampel, C.; Werner, H.-J. Coupled Cluster Theory for High Spin, Open Shell Reference Wave Functions. *J. Chem. Phys.* **1993**, *99*, 5219−5227.

(36) Knizia, G.; Adler, T. B.; Werner, H.-J. Simplified CCSD(T)-F12 Methods: Theory and Benchmarks. *J. Chem. Phys.* **2009**, *130*, 054104.

(37) Werner, H.-J.; Knowles, P. J.; Knizia, G.; Manby, F. R.; Schütz, M.; et al. *Molpro*, version 2015.1, a package of ab initio programs; see http://www.molpro.net.

(38) Xie, J.; Sun, R.; Siebert, M. R.; Otto, R.; Wester, R.; Hase, W. L. Direct Dynamics Simulations of the Product Channels and Atomistic Mechanisms for the $OH^- + CH_3I$ Reaction. Comparison with Experiment. *J. Phys. Chem. A* **2013**, *117*, 7162−7178.

DOI: 10.1021/acs.jpca.7b11927
J. Phys. Chem. A 2018, 122, 1886−1895

(39) Xie, J.; McClellan, M.; Sun, R.; Kohale, S. C.; Govind, N.; Hase, W. L. Direct Dynamics Simulation of Dissociation of the $[CH_3–I–OH]^-$ Ion−Molecule Complex. *J. Phys. Chem. A* **2015**, *119*, 817−825.
(40) Szabó, I.; Czakó, G. Double-Inversion Mechanisms of the X^- + CH_3Y [X,Y = F, Cl, Br, I] S_N2 Reactions. *J. Phys. Chem. A* **2015**, *119*, 3134−3140.
(41) Zhang, J.; Xie, J.; Hase, W. L. Dynamics of the F^- + CH_3I → HF + CH_2I^- Proton Transfer Reaction. *J. Phys. Chem. A* **2015**, *119*, 12517−12525.
(42) Lee, T. J.; Taylor, P. R. A Diagnostic for Determining the Quality of Single-Reference Electron Correlation Methods. *Int. J. Quantum Chem.* **1989**, *36*, 199−207.
(43) Czakó, G.; Szabó, I.; Telekes, H. On the Choice of the ab Initio Level of Theory for Potential Energy Surface Developments. *J. Phys. Chem. A* **2014**, *118*, 646−654.
(44) Ma, Y.-T.; Ma, X.; Li, A.; Guo, H.; Yang, L.; Zhang, J.; Hase, W. L. Potential Energy Surface Stationary Points and Dynamics of the F^- + CH_3I Double Inversion Mechanism. *Phys. Chem. Chem. Phys.* **2017**, *19*, 20127−20136.

DOI: 10.1021/acs.jpca.7b11927
J. Phys. Chem. A 2018, 122, 1886−1895